

Towards in situ determination of 3D strain and reorientation in the interpenetrating nanofibre networks of cuticle

Yi Zhang^{a,b,∇}, Paolino-De Falco^{a,∇}, Yanhong Wang^a, Ettore Barbieri^a, Oskar Paris^c, Nick Terrill^d, Gerald Falkenberg^b, Nicola Pugno^{e,a,f} and Himadri S. Gupta^{*a}

∇: These authors contributed equally to this work

Section 1: Cuticle structure and diffraction geometry:

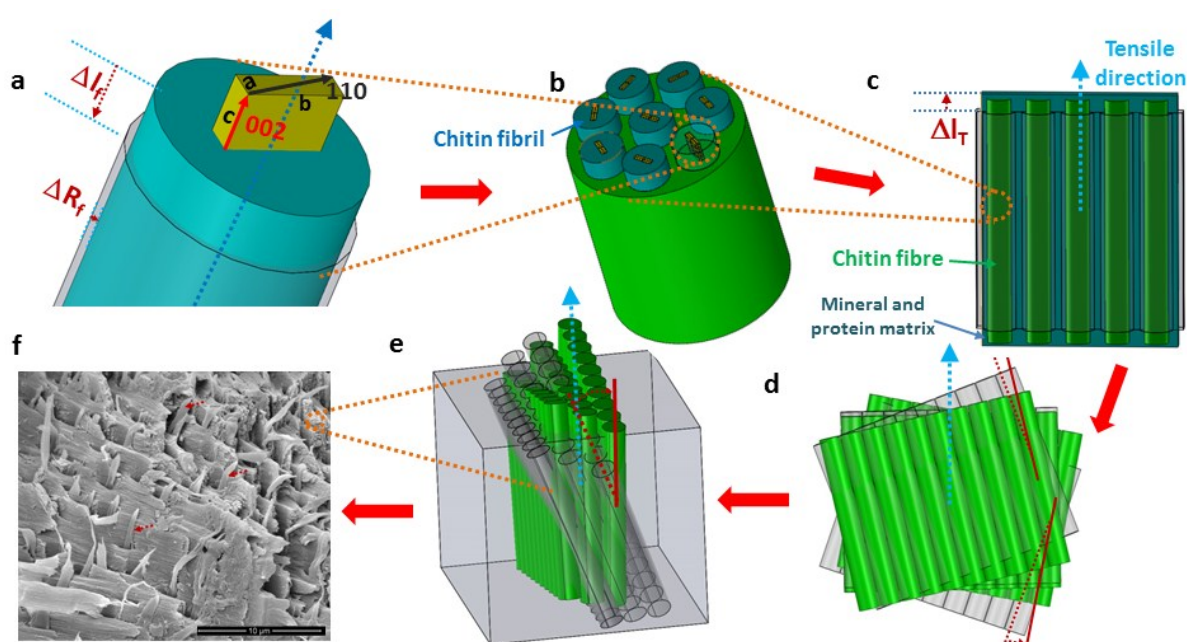


Figure S1. Hierarchical structure of stomatopod cuticle and corresponding mechanical parameters. (a) Schematic of a chitin fibre which is formed by N-acetyl-glucosamine molecules arranged in an orthorhombic crystal structure and proteins. (b) A mineralized chitin fibre which contains multiple fibres arranged in random orientations. The c axis of the chitin unit cell is coincided with both of the fibril and fibre axis which can be used as a proxy of the axial deformation of the chitin nanofibres. (c) The deformation of the fibre plane composed of parallel-arranged chitin fibres surrounded by protein and mineral matrix. (d) Schematic shows the in-plane rotation of mineralized chitin fibres due to external tensile load. (e) Schematic showing 3D fibre plane tilting due to external tensile load. (f) Scanning electron micrograph showing the plywood structure of in-plane chitin fibres is interrupted by the out-of-plane fibres running through the pore-canal system in the cuticle.

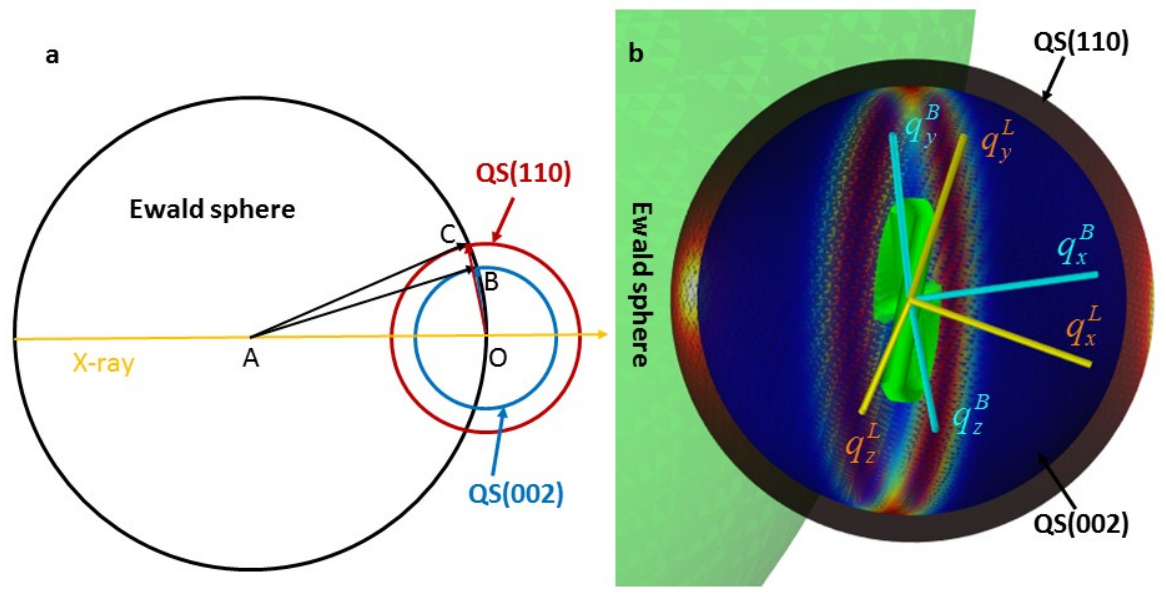


Figure S2. Ewald construction for (110) and (002) reflections in 2D and 3D. (a) Two-dimensional drawing of Ewald sphere construction with the reciprocal space intensity spheres for (110) and (002), denoted $QS(110)$ and $QS(002)$ respectively. The length of $AC=AO$ is $2\pi/\lambda$. Point C and B are located on the intersection ring between Ewald sphere and $QS(110)$, $QS(002)$ respectively. OC indicates the scattering vector q for (110) reflection, and OB the scattering vector for (002) reflection. (b) Three-dimensional rendering of the geometry in (a), showing the Ewald sphere intersection with $QS(110)$ and $QS(002)$ in 3D. The uniform initial fibre distribution in the Bouligand layer leads to a uniform band of (002) diffraction intensity in the vertical plane (red-orange in the figure).

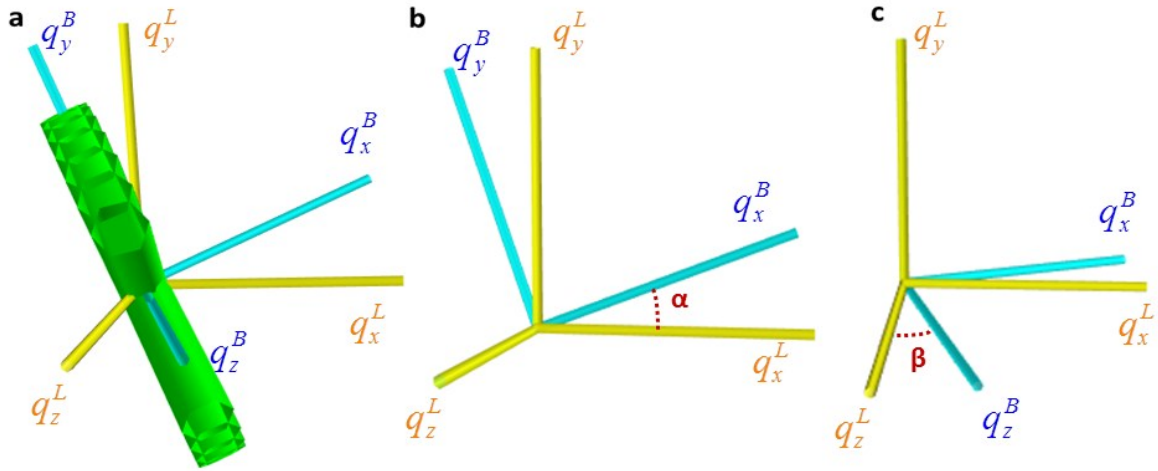


Figure S3. Linear transformation matrix between body-fixed frame and lab-fixed frame. (a) Schematic plot showing a fibre plane is tilted in 3D in the lab-fixed frame (yellow) while the plane is fixed in its body-fixed coordinate system (blue). (b-c) Schematic plot showing α (b) tilt and β (c) tilt of the body-fixed coordinate system from the body-fixed coordinate system.

The linear transformation matrix which translates coordinates (q_x^B, q_y^B, q_z^B) from body-fixed frame into laboratory-fixed coordinates (q_x^L, q_y^L, q_z^L) can be expressed by the following equation:

$$\begin{pmatrix} q_x^L \\ q_y^L \\ q_z^L \end{pmatrix} = \begin{pmatrix} \cos(\alpha)\cos(\beta) & -\sin(\alpha)\cos(\beta) & \sin(\beta) \\ \sin(\alpha) & \cos(\alpha) & 0 \\ -\cos(\alpha)\sin(\beta) & \sin(\alpha)\sin(\beta) & \cos(\beta) \end{pmatrix} \begin{pmatrix} q_x^B \\ q_y^B \\ q_z^B \end{pmatrix} \quad \text{Eq. S1}$$

Section 2: X-ray Diffraction Model Functions:

Table 1: Mathematical functions for intensity distributions on the QS(110) and QS(002) spheres and the corresponding intersection rings.

I: Delta functions (without 3D tilt):

In the formulae following, we have modelled the diffraction intensity of rings or spots on the reciprocal

spheres using peaked Gaussians which approach Dirac δ -functions as $\Delta q_{x(002)} \rightarrow 0$ ¹. In the following, the angle γ refers to the angle of the fibre in the q_y - q_z plane of **Fig 2b** (main text). The Bouligand lamellar unit lies in that plane, so a fibre at angle γ refers to the fibres in the sublamella (lamina) inclined at an angle γ in the Bouligand unit. In the L2 geometry, γ is replaced by α (Eq. s4). In evaluating the asymptotic limit to the integral, the relation $\delta(f(x)) = \delta(x)/|f'(x_0)|$ with x_0 a root of the function $f(x)$ is also used, which accounts for the denominator in some of the terms.

Configuration	Reflection	Function
L1	110	$\delta_{(110)}^{L1} = \frac{1}{\sqrt{2\pi}\Delta q_{(110)}} \exp\left(-\frac{1}{2}\left(\frac{q_y \cos \gamma + q_z \sin \gamma}{\Delta q_{(110)}}\right)^2\right)$ Eq. s2
L1	002	$\delta_{(002)}^{L1} = \frac{1}{\sqrt{2\pi}\Delta q_{(002)}} \frac{\exp\left(-\frac{1}{2}\left(\frac{q_x}{\Delta q_{(002)}}\right)^2\right)}{\sqrt{(q_{(002)})^2 - (q_x)^2}}$ Eq. s3
L2	110	$\delta_{(110)}^{L2} = \frac{1}{\sqrt{2\pi}\Delta q_{(110)}} \exp\left(-\frac{1}{2}\left(\frac{q_y \cos \alpha + q_x \sin \alpha}{\Delta q_{(110)}}\right)^2\right)$ Eq. s4
L2	002	$\delta_{(002)}^{L2} = \frac{1}{\sqrt{2\pi}\Delta q_{(002)}} \frac{\exp\left(-\frac{1}{2}\left(\frac{q_z}{\Delta q_{(002)}}\right)^2\right)}{\sqrt{(q_{(002)})^2 - (q_z)^2}}$ Eq. s5

II: Weight functions for the fibre distribution before mechanical loading:

The weight functions will change on mechanical loading. The changes of weight functions and $I(\chi)$ with the tissue strain (ϵ_T) for (002) reflection under L1 configuration are described later in the *Supplementary Information* in Section 4).

Configuration	Fibre group	Function
L1	IP	$w_0 = 1/\pi$ Eq. s6
L1	OP	$w(\gamma; \gamma_0, \Delta\gamma_0) = \frac{1}{\sqrt{2\pi}\Delta\gamma_0} \exp\left(-\frac{1}{2}\left(\frac{\gamma - \gamma_0}{\Delta\gamma_0}\right)^2\right)$ Eq. s7
L2	IP	$w(\alpha; \alpha_{IP}, \Delta\alpha_{IP}) = \frac{1}{\sqrt{2\pi}\Delta\alpha_{IP}} \exp\left(-\frac{1}{2}\left(\frac{\alpha - \alpha_{IP}}{\Delta\alpha_{IP}}\right)^2\right)$ Eq. s8
L2	OP	$w(\alpha; \alpha_{OP}, \Delta\alpha_{OP}) = \frac{1}{\sqrt{2\pi}\Delta\alpha_{OP}} \exp\left(-\frac{1}{2}\left(\frac{\alpha - \alpha_{OP}}{\Delta\alpha_{OP}}\right)^2\right)$ Eq. s9
III: Coordinates on the intersection ring		
Reflection	Function	
110	$q_x^{110} = -\frac{q_{(110)}^2}{2q_{(ES)}}$ $q_y^{110} = \frac{q_{(110)}}{2q_{(ES)}} \sqrt{(2q_{(ES)} + q_{(110)})(2q_{(ES)} - q_{(110)})} \sin \chi$ Eq. s10 $q_z^{110} = \frac{q_{(110)}}{2q_{(ES)}} \sqrt{(2q_{(ES)} + q_{(110)})(2q_{(ES)} - q_{(110)})} \cos \chi$	
002	$q_x^{002} = -\frac{q_{(002)}^2}{2q_{(ES)}}$ $q_y^{002} = \frac{q_{(002)}}{2q_{(ES)}} \sqrt{(2q_{(ES)} + q_{(002)})(2q_{(ES)} - q_{(002)})} \sin \chi$	

$$q_z^{002} = \frac{q_{(002)}}{2q_{(ES)}} \sqrt{(2q_{(ES)} + q_{(002)})(2q_{(ES)} - q_{(002)})} \cos \chi$$

Eq. s11

IV: Delta functions with 3D tilt

$$\delta_{(110)}^{L1}(q_x, q_y, q_z; \gamma, \Delta q_{(110)}, \alpha, \beta) = \frac{1}{\sqrt{2\pi}\Delta q_{(110)}} \exp\left(-\frac{1}{2}\left(\frac{(q_x \sin \alpha + q_y \cos \alpha) \cos \gamma + (-q_x \cos \alpha \sin \beta + q_y \sin \alpha \sin \beta + q_z \cos \beta) \sin \gamma}{\Delta q_{(110)}}\right)^2\right)$$

Eq. s12

$$\delta_{(002)}^{L1}(q_x, q_y, q_z; \gamma, \Delta q_{(002)}, \alpha, \beta) = \frac{1}{\sqrt{2\pi}\Delta q_{(002)}} \exp\left(-\left(\frac{q_x \cos \alpha \cos \beta - q_y \sin \alpha \cos \beta + q_z \sin \beta}{\Delta q_{(002)}}\right)^2\right) \frac{1}{\sqrt{(q_{(002)})^2 - (q_x \cos \alpha \cos \beta - q_y \sin \alpha \cos \beta + q_z \sin \beta)^2}}$$

Eq. s13

$$\delta_{(110)}^{L2}(q_x, q_y, q_z; \gamma, \Delta q_{(110)}, \alpha, \beta) = \frac{1}{\sqrt{2\pi}\Delta q_{(110)}} \exp\left(-\frac{1}{2}\left(\frac{(q_y \cos \gamma - q_z \sin \gamma) \cos \alpha + (-q_x \cos \beta + q_y \sin \gamma \sin \beta + q_z \cos \gamma \sin \beta) \sin \alpha}{\Delta q_{(110)}}\right)^2\right)$$

Eq. s14

$$\delta_{(002)}^{L2}(q_x, q_y, q_z; \gamma, \Delta q_{(002)}, \alpha, \beta) = \frac{1}{\sqrt{2\pi}\Delta q_{(002)}} \exp\left(-\left(\frac{q_x \sin \beta + q_y \sin \alpha \cos \beta + q_z \cos \alpha \cos \beta}{\Delta q_{(002)}}\right)^2\right) \frac{1}{\sqrt{(q_{(002)})^2 - (q_x \sin \beta + q_y \sin \alpha \cos \beta + q_z \cos \alpha \cos \beta)^2}}$$

Eq. s15

V: Intensity distribution on the intersection ring ($I(\chi)$):

The measured intensity is the integral of the diffraction intensities of each fibre (Section IV) weighted by the fibre orientation distribution (Section II).

Configuration	Reflection	Function
L1	110	$I_{110(\chi)}^{L1} = \lambda_{IP} \int_{-\frac{\pi}{2}}^{\frac{\pi}{2}} w_0 \times \delta_{(110)}^{L1}(q_x^{110}, q_y^{110}, q_z^{110}; \gamma, \Delta q_{(110)}, \alpha_{IP}, \beta_{IP}) d\gamma +$ $\lambda_{OP} \int_{-\frac{\pi}{2}}^{\frac{\pi}{2}} w(\gamma; \gamma_0, \Delta\gamma) \times \delta_{(110)}^{L1}(q_x^{110}, q_y^{110}, q_z^{110}; \gamma, \Delta q_{(110)}, \alpha_{OP}, \beta_{OP}) d\gamma$ <p style="text-align: center;">Eq. s16</p>
L1	002	$I_{002(\chi)}^{L1} = \lambda_{IP} \int_{-\frac{\pi}{2}}^{\frac{\pi}{2}} w_0 \times \delta_{(002)}^{L1}(q_x^{002}, q_y^{002}, q_z^{002}; \gamma, \Delta q_{(002)}, \alpha_{IP}, \beta_{IP}) d\gamma +$ $\lambda_{OP} \int_{-\frac{\pi}{2}}^{\frac{\pi}{2}} w(\gamma; \gamma_0, \Delta\gamma) \times \delta_{(002)}^{L1}(q_x^{002}, q_y^{002}, q_z^{002}; \gamma, \Delta q_{(002)}, \alpha_{OP}, \beta_{OP}) d\gamma$ <p style="text-align: center;">Eq. s17</p>
L2	110	$I_{110(\chi)}^{L2} = \lambda_{IP} \int_{-\frac{\pi}{2}}^{\frac{\pi}{2}} w(\alpha; \alpha_{IP}, \Delta\alpha_{IP}) \times \delta_{(110)}^{L2}(q_x^{110}, q_y^{110}, q_z^{110}; \gamma, \Delta q_{(110)}, \alpha_{IP}, \beta_{IP}) d\alpha$ $+ \lambda_{OP} \int_{-\frac{\pi}{2}}^{\frac{\pi}{2}} w(\alpha; \alpha_{OP}, \Delta\alpha_{OP}) \times \delta_{(110)}^{L2}(q_x^{110}, q_y^{110}, q_z^{110}; \gamma, \Delta q_{(110)}, \alpha_{OP}, \beta_{OP}) d\alpha$ <p style="text-align: center;">Eq. s18</p>
L2	002	$I_{002(\chi)}^{L2} = \lambda_{IP} \int_{-\frac{\pi}{2}}^{\frac{\pi}{2}} w(\alpha; \alpha_{IP}, \Delta\alpha_{IP}) \times \delta_{(002)}^{L2}(q_x^{002}, q_y^{002}, q_z^{002}; \gamma, \Delta q_{(002)}, \alpha_{IP}, \beta_{IP}) d\alpha$ $+ \lambda_{OP} \int_{-\frac{\pi}{2}}^{\frac{\pi}{2}} w(\alpha; \alpha_{OP}, \Delta\alpha_{OP}) \times \delta_{(002)}^{L2}(q_x^{002}, q_y^{002}, q_z^{002}; \gamma, \Delta q_{(002)}, \alpha_{OP}, \beta_{OP}) d\alpha$ <p style="text-align: center;">Eq. s19</p>

VI: Symbol definitions:

γ : The fibre orientation respect to the q_z^L axis in the lab coordinate system;

λ_{IP} : scaling factor proportional to amount of in-plane (IP) fibres in the scattering volume;

λ_{OP} : scaling factor proportional to amount of out-of-plane (OP) fibres in the scattering volume;

$q_{(ES)}$: The radius of Ewald sphere $2\pi/\lambda$ (AC in **Figure S2a**);

$q_{(002)}$: The radius of $QS(002)$ sphere (OB in **Figure S2a**);

$q_{(110)}$: The radius of $QS(110)$ sphere (OC in **Figure S2a**)

Section S3: Analytical results for coupled laminate deformation and reorientation of Bouligand layer

Overview: Classical lamination theory ² was used to analyze the fibre deformation and the fibre reorientation of the stomatopod cuticle. The plywood structure of the Bouligand layer was studied as a laminate, i.e. a stack of different orientated composite plies. The reinforcement (fibre) was considered to be the mineralized chitin fibre, and the continuous phase (matrix) was taken to be the mineral-protein composite. Both materials were assumed to behave in a linear elastic manner, i.e. the analytical formulation would be expected to be valid to the cuticle elastic limit of about ~0.6-0.8% tissue strain. Each plywood lamina was assumed to be orthotropic and to exist in a state of plane stress.

Material property assignment: The material properties of the components were taken from the literature ³. The chitin nanofibres were composed of a crystalline region of chitin ($E_{ch}= 60$ GPa, $\nu_{ch}= 0.25$, $\varphi_{ch}= 0.31$) and proteins ($E_{prf}= 56$ MPa, $\nu_{prf}= 0.28$, $\varphi_{prf}= 0.69$), whilst the mineral matrix is composed of amorphous calcium carbonate spherules ($E_{ACC}= 37$ GPa, $\nu_{ACC}= 0.35$, $\varphi_{ACC}= 0.9$) and different proteins ($E_{prm}= 570$ MPa, $\nu_{prf} = 0.28$, $\varphi_{prf} = 0.1$). Here, $E_{subscript}$ indicates the Young's modulus for the *subscript* phase, $\nu_{subscript}$ indicates the Poisson's modulus and $\varphi_{subscript}$ the volume fraction of the component. Chitin modulus was taken from ⁴.

The homogenized material properties of a single lamina were found by applying a rule of mixture (combination of Voigt and Reuss models) model twice – first at the fibrillar and the next time at the fibre level ².

At the fibrillar level, the Voigt model ⁵ was used to calculate the Young's moduli and Poisson coefficients of the chitin protein nanofibrils and of the mineral-protein matrix, using the volume fraction φ_{ch} listed above.

Secondly, we found the mechanical properties of the orthotropic lamina (**Fig S4**) as standard for a composite material ², by (a) using the Voigt model to obtain the Young's modulus E_1 along the fibre direction (direction 1 in **Fig S4** parallel to fibre direction) and the Poisson's constant ν_{12} , and (b) obtaining the Young's modulus E_2 and the shear modulus G_{12} perpendicular to the fibre direction (direction 2 in **Fig S4**), with the Reuss model.

We calculated the shear moduli of the fibre and of the matrix (G_{fibre} and G_{matrix}) by using the expression valid for isotropic linear elastic material:

$$G = \frac{E}{2(1+\nu)} \text{ Equation s20}$$

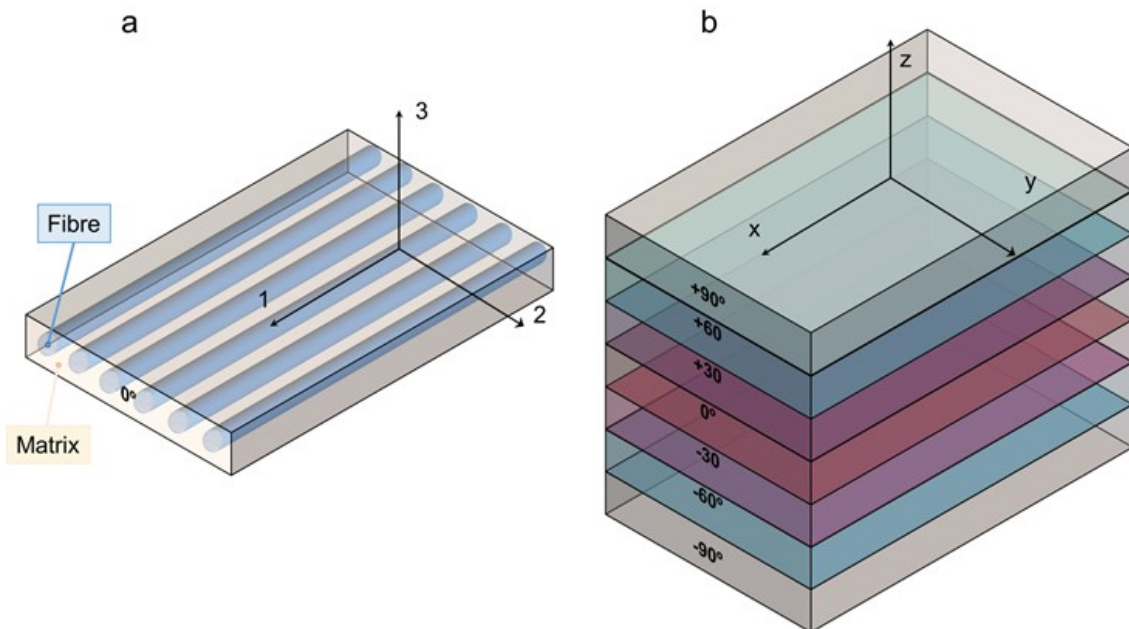


Figure S4. Laminate composite model. (a) Schematic figure showing a single lamina made of fibres aligned along the direction 1 and embedded in a matrix. The thickness of each lamina is 0.1 μm . (b) Schematic figure of a plywood laminate. A quasi-continuously orientated structure made of 100 laminae (only 7 laminae were shown

for convenience) is used for the analyses. The rotational angle between consecutive laminae considered for the analysis is 1.8 degrees.

After calculating the homogenized material properties for the lamina, we approximated the experimental Bouligand structure by applying the lamination theory to a 10 μm thick laminate ⁶, containing 100 laminae with an angular quasi-continuous distribution of plies (1.8 degrees between two consecutive laminae, from -90° to 90°).

The main formula which links the loading to the deformation state of the laminate is shown below:

$$\begin{bmatrix} N \\ M \end{bmatrix} = \begin{bmatrix} A & B \\ B & D \end{bmatrix} \begin{bmatrix} \varepsilon \\ \kappa \end{bmatrix} \quad \text{Equation s21}$$

Where N represents the 2 uniaxial forces (N_x and N_y) and the shear N_{xy} acting in the plane of the laminate (directions x-y), M_x and M_y the 2 static moments acting along directions x-y, and the torque M_{xy} . $[A]$, $[B]$ and $[D]$ are the stiffness matrices of the laminate, while $[\varepsilon]$ represents the strains and $[\kappa]$ the curvatures of the laminate.

Under the assumptions of lamination theory ² the curvatures are neglected, and with $[N] = (N_x, 0, 0)$ as the experimental load for uniaxially applied tension, we find the laminate strains from Equation. S21.

$$[\varepsilon] = [A]^{-1} \cdot [N] \quad \text{Equation s22}$$

$[A]$ can be calculated with the formula:

$$A_{ij} = \sum_{k=1}^n [Q]_{ij}^k (h_k - h_{k-1}) \quad \text{Equation s23}$$

Where the matrix $[Q]_{ij}$ is the assembled matrix of the laminate and h_k represents the distance of the k^{th} lamina from the mid-plane of the laminate. Once the laminate strains are obtained, the strain vectors in each A_{ij} lamina frame is calculated by multiplying $[\varepsilon]$ with the transformation matrix $[T]$:

$$[T] = \begin{bmatrix} \cos^2 \theta & \sin^2 \theta & \cos \theta \sin \theta \\ \sin^2 \theta & \cos^2 \theta & -\cos \theta \sin \theta \\ -2 \cos \theta \sin \theta & 2 \cos \theta \sin \theta & \cos^2 \theta - \sin^2 \theta \end{bmatrix} \quad \text{Equation s24}$$

Calculation of in-plane reorientation: The reorientation was calculated as lamina shear strain divided by 2, as per the **Figure S5**, a result which is also confirmed by finite element simulation. Analytically, this results in the expression for angular reorientation $\Delta\gamma(\sigma_{xx})$ (the factor 2 arises from the tensorial definition of strain compared to engineering strain):

$$\Delta\gamma(\sigma_{xx}) = \frac{\epsilon_{12}}{2} \quad \text{Equation s25}$$

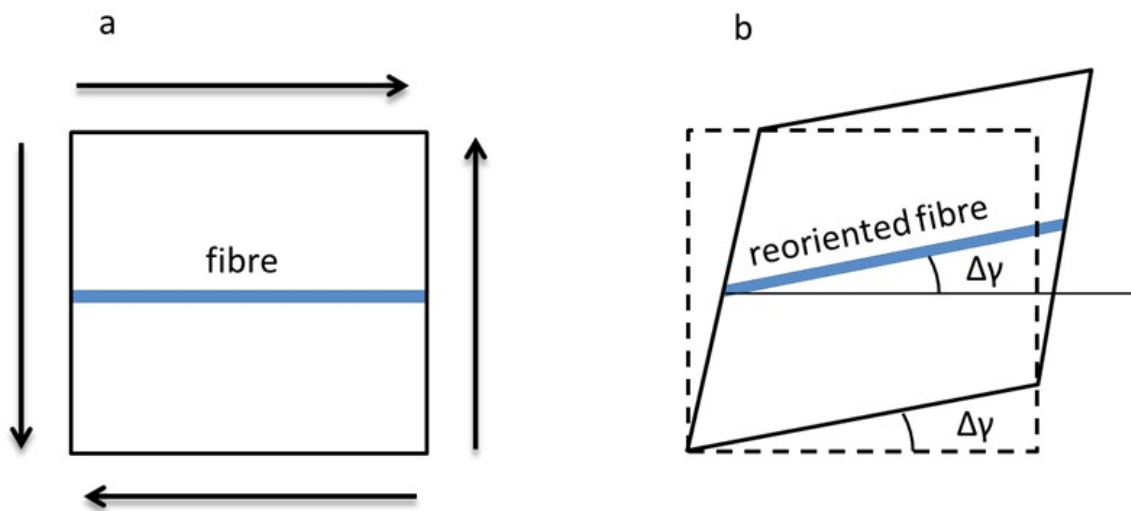


Figure S5. In-plane angular reorientation of lamina under shear strain. a) Undeformed configuration. b) Deformed configuration. Dashed line is used for undeformed configuration. We calculated the fibre reorientation $\Delta\gamma$ as $\epsilon_{12}/2$, where ϵ_{12} is the engineering shear strain in the hypotheses of small displacements. All the strain components are rotated in the reference frame of each lamina. Hence, the strain components along and perpendicular to the fibres direction do not contribute to reorientation.

Section S4. Calculation of changed orientation function (in-plane) upon fibre reorientation:

Consider a small angular sector of fibres (e.g. within one lamina). The number of fibres is $w(\gamma; \gamma_0, \Delta\gamma_0)\Delta\gamma$ (up to normalization constants). Under deformation, this sector moves to a new angular position γ_σ and also changes in width $\Delta\gamma_\sigma$ (e.g. under tensile load, γ will move closer to loading direction and the width will reduce). Most importantly, the fibre distribution will also change from $w(\gamma; \gamma_0, \Delta\gamma_0)$ to $w_\sigma(\gamma; \gamma_0, \sigma, \Delta\gamma_0, \sigma)$ (**Fig 3f**), where the parameters in the second term represent the centre and width of the modified distribution, and do not imply the same functional form as $w(\gamma; \gamma_0, \Delta\gamma_0)$. Therefore, as no fibres are created or destroyed, we have

$$w(\gamma; \gamma_0, \Delta\gamma_0)\Delta\gamma = w_\sigma(\gamma; \gamma_0, \sigma, \Delta\gamma_0, \sigma)\Delta\gamma_\sigma \quad \text{Equation s26}$$

As the change in angle is expected to be proportional (to first order) to the perturbing parameter (stress), we can write

$$\gamma_\sigma = \gamma - \tilde{\sigma}f(\gamma) \quad \text{Equation s27}$$

Where $f(\gamma)$ is an a priori unknown function and we have scaled the stress variable by a large parameter (100 MPa that is a value close to the maximum applied stress) to obtain a dimensionless stress parameter $\tilde{\sigma} = \left(\frac{\sigma}{\sigma_0}\right)$.

Substituting in the equations above we get, using first order perturbation expansions ¹ where $w(\gamma; \gamma_0, \Delta\gamma_0)$ and $w_\sigma(\gamma; \gamma_0, \sigma, \Delta\gamma_0, \sigma)$ is written in shorthand below as $w(\gamma)$ and $w_\sigma(\gamma)$ to keep the equation on one line (the variable is γ throughout):

$$w_\sigma(\gamma) \approx w(\gamma) + \tilde{\sigma} \left(f(\gamma) \frac{dw}{d\gamma} + w(\gamma) \frac{df}{d\gamma} \right) = w(\gamma) + \tilde{\sigma} \frac{d(f(\gamma)w(\gamma))}{d\gamma} \quad \text{Equation s28}$$

In cuticle, we start with a uniform fibril distribution $w(\gamma; \gamma_0, \Delta\gamma_0) = w_0 = 1/\pi$ to get

$$w_\sigma(\gamma; \gamma_0, \Delta\gamma_0) \approx w_0 \left(1 + \tilde{\sigma} \frac{df}{d\gamma} \right) \quad \text{Equation s29}$$

From the lamination theory we found:

$$f(\gamma) = \frac{(-2 \cos \theta \sin \theta \varepsilon_x + 2 \cos \theta \sin \theta \varepsilon_y + \gamma_{xy} \cos^2 \theta - \gamma_{xy} \sin^2 \theta)}{2} \quad \text{Equation s30}$$

Simplifying the **Equation 29** we obtain:

$$f(\gamma) \approx A \cos 2\gamma + B \sin 2\gamma \text{ Equation s31}$$

Where $A = \frac{\gamma_{xy}}{2}$ and $B = \frac{(\varepsilon_y - \varepsilon_x)}{2}$ are constants depending on the material parameters of the chitin, mineral and protein components of the cuticle. Using this form, we have the final result

$$w_\sigma(\gamma; \gamma_0, \Delta\gamma_0) \approx w_0(1 + 2\tilde{\sigma}(-A \sin 2\gamma + B \cos 2\gamma)) \text{ Equation s32}$$

It is possible to show from **Equation s22** that the element in the matrix $[A]^{-1}$ which couples the laminate shear strain γ_{xy} and the applied uniaxial load N_x is null. Hence, $A = 0$ while $B = -2.28 \times 10^{-3} \times \tilde{\sigma}$ [no units]. γ is equivalent to the azimuthal angle χ here.

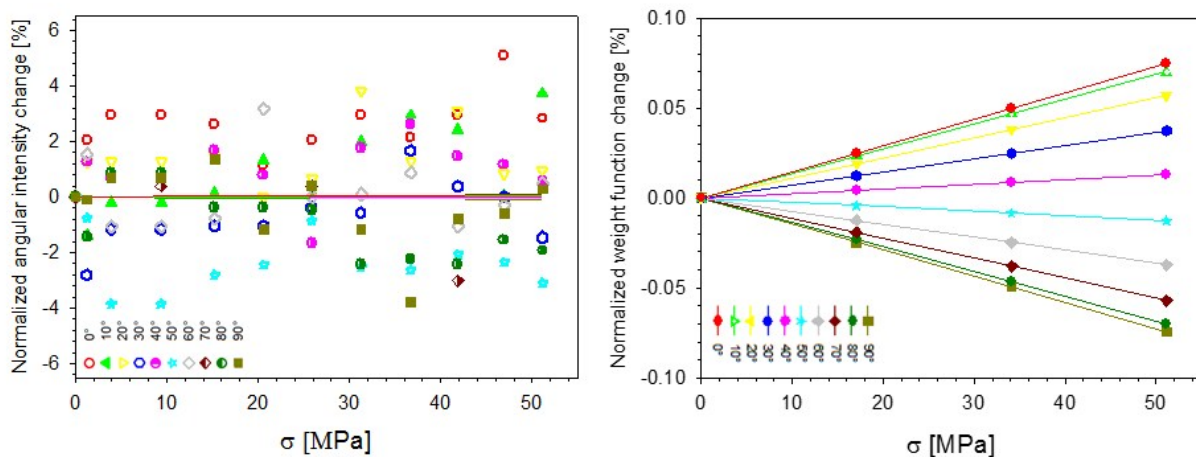


Figure S6. Angularly-resolved changes in experimental and simulated fibril weight function with respect to tensile stress. a) Percentage changes in intensity in different angular sectors (different colours) with increasing applied tensile stress, normalized at each stress-level to the total area under the $I(\chi)$ plot (to account for any residual intra-sample material heterogeneity encountered when translating the sample with respect to the beam between each stress-level). The angles are measured in terms of $\psi = 90^\circ - \chi$, i.e. $\psi=0^\circ$ corresponds to vertical direction (parallel to direction of applied load). For a planar lamella with zero tilt ($\alpha=\beta=0^\circ$), the normalized angular intensity profile is proportional to the fibril weight function (b) Percentage changes in fibril weight function, using the laminate model described above. It is observed that the changes are far smaller than the observed changes in (a), indicating that effects from tilting (nonzero α and β) must be considered.

Supplementary References:

1. C. M. Bender and S. A. Orszag, *Advanced mathematical methods for scientists and engineers*, Springer, New York, 1999.
2. J.-M. Berthelot, in *Composite Materials: Mechanical Behavior and Structural Analysis*, ed. J.-M. Berthelot, Springer New York, New York, NY, 1999, DOI: 10.1007/978-1-4612-0527-2_14, pp. 287-311.
3. S. Nikolov, H. Fabritius, M. Friak and D. Raabe, *Bulgarian Chemical Communications*, 2015, **47**, 423-432.
4. Y. Ogawa, R. Hori, U.-J. Kim and M. Wada, *Carbohydrate Polymers*, 2011, **83**, 1213-1217.
5. D. Hull and T. W. Clyne, *An introduction to composite materials*, Cambridge University Press, Cambridge, UK, 2nd edition edn., 1996.
6. D. Raabe, C. Sachs and P. Romano, *Acta Materialia*, 2005, **53**, 4281-4292.